

Quantum interference of single photons from remote nitrogen-vacancy centers in diamond

A. Sipahigil,¹ M. L. Goldman,¹ E. Togan,¹ Y. Chu,¹ M. Markham,²
D. J. Twitchen,² A. S. Zibrov,¹ A. Kubanek,^{1,*} and M. D. Lukin¹

¹*Department of Physics, Harvard University, Cambridge, Massachusetts 02138, USA*

²*Element Six Ltd, Kings Ride Park, Ascot SL5 8BP, UK*

We demonstrate quantum interference between indistinguishable photons emitted by two nitrogen-vacancy (NV) centers in distinct diamond samples separated by two meters. Macroscopic solid immersion lenses are used to enhance photon collection efficiency. Quantum interference is verified by measuring a value of the second-order cross-correlation function $g^{(2)}(0) = 0.34 \pm 0.04 < 0.5$. In addition, optical transition frequencies of two separated NV centers are tuned into resonance with each other by applying external electric fields. Extension of the present approach to generate entanglement of remote solid-state qubits is discussed.

The interference of two identical photons impinging on a beamsplitter leads to perfect coalescence where both photons leave through the same output port. This fundamental effect, known as Hong-Ou-Mandel (HOM) interference [1], is a consequence of bosonic statistics for indistinguishable particles. HOM interference has been demonstrated using single photon pairs from parametric down-conversion [2] and delayed photons from a single photon source [3–5]. HOM interference has recently drawn attention as a resource for entanglement generation between distinct single-photon emitters with many potential applications in quantum information science [6]. The effect has been observed for photons emitted by pairs of atoms [7] and trapped ions [8], and has been used for entanglement generation of remote trapped ions [9]. While isolated atoms and ions, which are nominally identical, are a natural source of indistinguishable photons, extending these ideas to condensed matter systems can be challenging since two solid-state emitters are generally distinguishable because of their different local environments. This Letter demonstrates quantum interference of two photons produced by nitrogen-vacancy (NV) impurities in distinct diamond samples separated by two meters. Complementing the recent work involving other solid-state systems [10–13], the present solid-state realization is particularly significant, since electronic and nuclear spins associated with NV centers can be used as a robust solid-state qubit memory, yielding potential scalable architectures for quantum networks [14, 15]. Specifically, in combination with a recent demonstration of spin-photon entanglement [16], the present work paves the way for entanglement generation between remote solid-state qubits.

Unlike those associated with atoms in free space, the optical properties of NV centers embedded in a solid state vary substantially from emitter to emitter, especially in distinct samples. This inhomogeneity is due to variation in the local environments of NV centers and, in particular, to variation in the local strain. Furthermore, coincidence experiments are limited by the collection efficiency

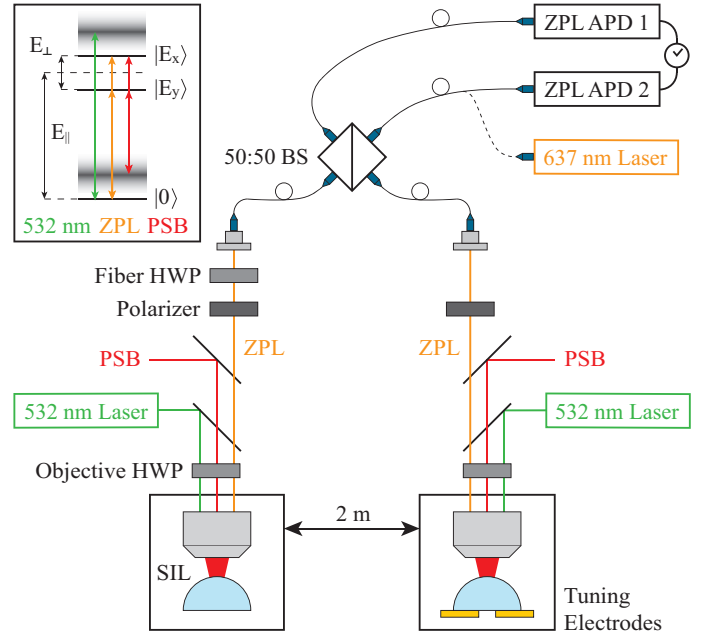


FIG. 1. Schematic of the apparatus. Two diamond SILs containing multiple NV centers are housed in continuous helium flow cryostats 2 m apart. Each SIL is addressed by a separate confocal microscopy setup, which includes an arm for excitation at 532 nm, a collection arm for the phonon sideband (PSB), and a collection arm for the zero-phonon line (ZPL). The ZPL collection arm is coupled through a half-wave plate (HWP) into a polarization-maintaining single-mode 50:50 fiber beamsplitter. The two beamsplitter output arms are connected to a pair of avalanche photodiodes (APDs), completing the Hanbury Brown and Twiss detection setup. An excitation laser at 637 nm is connected in place of ZPL APD 2 to acquire the absorption scan spectra. Electrodes for electric field tuning are installed in one cryostat. The inset shows a simplified level structure, including non-resonant excitation into the excited state PSB at 532 nm, emission into the ground state PSB, and resonant excitation and emission into the ZPL at 637 nm.

for light emitted by the NV center. While a wide variety

of approaches are currently being explored to enhance the collection efficiency [17–20], we here utilize solid immersion lenses (SILs) fabricated from bulk diamond [21] to facilitate the efficient collection of narrowband photons with identical properties from distant diamond samples. The SILs improve the collection efficiency in the relevant frequency range by an order of magnitude by minimizing total internal reflection at the air-diamond interface, which is significant because of the high refractive index ($n_d = 2.4$) of the diamond host. Very recently, microfabricated SILs have been used to observe HOM interference from two NV centers separated by roughly $20\ \mu\text{m}$ on the same diamond chip [10].

In our experiment, we use two 1.0-mm diameter SILs that are fabricated from bulk electronic grade diamond and cut along the (100) crystal plane. The SILs are placed in continuous flow helium cryostats that are separated by two meters, as shown in Fig. 1. Resonant excitation with an external-cavity diode laser at 637 nm and fluorescence detection of PSB emission reveal linewidths in the range of 50–250 MHz for individual transitions of NV centers in both SILs. These are comparable to narrowest linewidths observed in both synthetic and natural bulk diamond samples [22, 23].

To obtain identical photons from two NV centers, the NV centers need to have transitions that are spectrally overlapping, and the emission from these individual transitions for each NV needs to be isolated. By performing simultaneous absorption scans on NV centers in the two SILs with a single laser, we can directly measure the relative detuning of their optical transitions. In our experimental sequence, a $5\ \mu\text{s}$ pulse of green light initializes the NV center into the electronic spin sublevel of the triplet ground state with $m_s = 0$ ($|0\rangle$) [24]. Therefore, we only collect fluorescence from the NV center when the laser is resonant with transitions from the $|0\rangle$ state to the $|E_x\rangle$ or $|E_y\rangle$ states, as shown in inset of Fig. 1 [25]. We select a pair of NV centers such that one transition in the first NV center is resonant with one transition in the second.

For the HOM measurement, we excite the NV centers with green light and we want to collect ZPL emission only from the selected pair of resonant transitions. The linear and orthogonal polarization selection rules of the $|0\rangle \leftrightarrow |E_x\rangle$ and $|0\rangle \leftrightarrow |E_y\rangle$ transitions allow us to select the emission from one of these transitions by inserting linear polarizers into the ZPL collection arms [22] and setting the Objective HWP, shown in Fig. 1, to the correct angles. Because the ZPL collection used to measure the HOM interference and the resonant excitation used to perform the absorption scans follow the same optical path, we can use the absorption scans to set the correct polarization angle for the ZPL collection. Therefore, we can selectively collect photons emitted from the desired transitions under non-resonant excitation with green light.

We next demonstrate control over the optical proper-

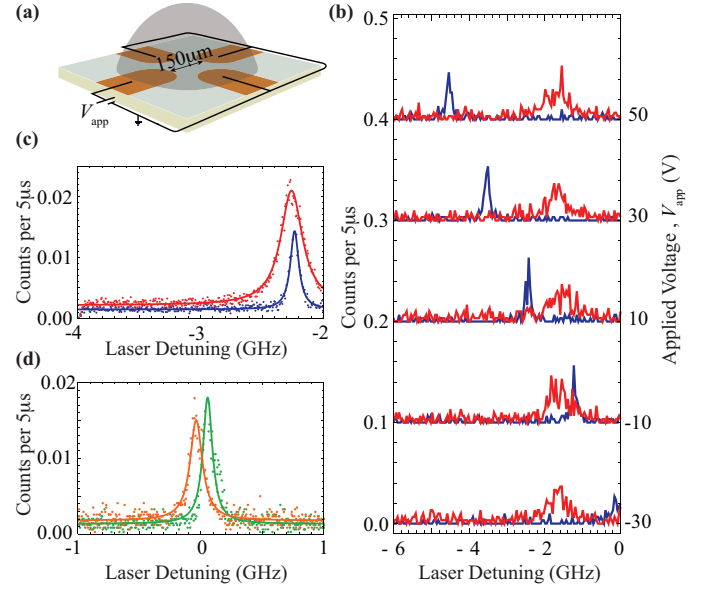


FIG. 2. Electric field tuning of optical transitions. (a) Four Cr/Au gates deposited on silicon. The central gap has a diameter of $150\ \mu\text{m}$. In this experiment, only one of the gate voltages was swept while the others were kept grounded. (b) Absorption scans for different applied gate voltages. The gate voltage V_{app} is varied from -30 to 50 V for NV1. The $|0\rangle \leftrightarrow |E_x\rangle$ transition of NV1 (blue) is tuned across the $|0\rangle \leftrightarrow |E_x\rangle$ transition of NV2 (red). For different V_{app} , absorption scan plots are offset by 0.1 for clarity. (c) Linewidth measurement under electric field tuning. On resonance, the measured linewidths are $85 \pm 2\ \text{MHz}$ for NV1 (blue) and $217 \pm 4\ \text{MHz}$ for NV2 (red). The detuning of the optical transitions in two samples is $25 \pm 2\ \text{MHz}$. (d) Linewidth measurement for the NV centers used for the HOM measurement. The measured linewidths are $88 \pm 3\ \text{MHz}$ (green) and $106 \pm 4\ \text{MHz}$ (orange), and the detuning is $93 \pm 10\ \text{MHz}$ without electric field tuning.

ties of NV pairs to compensate for strain-induced spectral inhomogeneities. We make use of the DC Stark effect to actively tune the selected transitions into resonance [23, 26]. Electric fields perpendicular to the NV axis vary the splitting between $|E_x\rangle$ and $|E_y\rangle$ states and parallel fields shift both transitions together, as shown in the inset of Fig. 1. This allows complete control over the optical transition frequencies [26, 27]. In order to apply the desired electric field, we place one of the SILs on top of a silicon wafer deposited with four electrodes, comprised of 40 nm Au on a Cr adhesion layer. The gate geometry is shown in Fig. 2(a). We apply a bias voltage, V_{app} , on one of the electrodes while keeping the other three grounded. In Fig. 2(b), the $|0\rangle \leftrightarrow |E_x\rangle$ transition of NV1 (blue) is tuned across the $|0\rangle \leftrightarrow |E_x\rangle$ transition of NV2 (red) by varying the applied voltage V_{app} from -30 V to 50 V. At $V_{\text{app}} = -2.9\ \text{V}$, shown in Fig. 2(c), the detuning between the two transitions is reduced to

25 MHz from an initial value of 270 MHz. We measured linewidths of 85 MHz for NV1, which was tuned, and 217 MHz for NV2, which was not tuned. Similarly, we did not observe a systematic change of the linewidths with applied external fields in several other NV centers.

Electric field tuning, however, limits the duty cycle when used in combination with green excitation. Here, the green excitation ionizes charge traps in the diamond lattice [26], and these charge dynamics limit the duty cycle during which we can collect fluorescence at the tuned frequency to 50%. For this reason, for the HOM measurement we selected NV centers whose transitions, shown in Fig. 2(d), are inherently detuned by 93 ± 10 MHz with linewidths of 88 ± 3 MHz and 106 ± 4 MHz, which eliminates the need for electric field tuning and allows us to run the experiment without reducing the duty cycle.

For the HOM interference measurement, we apply CW excitation at 532 nm to the two NV centers whose absorption spectra are shown in Fig. 2(d). To confirm that we are addressing one single-photon emitter in each SIL, we infer the normalized, second-order autocorrelation function $g_{\text{PSB}}^{(2)}(\tau)$ in a standard Hanbury Brown and Twiss setup by splitting the PSB emission in a 50:50 beamsplitter. We expect $g_{\text{PSB}}^{(2)}(0) = 0$ for an ideal single-photon source, and the single-photon nature of the emission is confirmed in Figs. 3(a,b). We ensure that the ZPL emission from the two NV centers is indistinguishable in frequency through spectral and polarization filtering, as described above. The filtered emission from each NV center is sent to an individual input port of a polarization-maintaining fiber-based beamsplitter. We balance the emission intensity by adjusting the green excitation intensity for each NV center independently to obtain 1100 counts per second (cps) per emitter at each output port of the beamsplitter. An additional HWP in one setup is used to adjust the polarization matching of the photons at the beamsplitter. The output ports of the beamsplitter are connected to single photon detectors with timing resolution below 100 ps. The cross-correlation between these detectors is evaluated using a Time-Correlated Single Photon Counting Module with a resolution of 64 ps.

We use the approach described in [11] to analyze the interference data presented in Figs. 3(c,d). The expected form of the two-emitter cross-correlation function, $g^{(2)}(\tau)$, is determined by the autocorrelation functions $g_{\text{PSB}}^{(2)}(\tau)$ of the individual emitters, the signal-to-noise ratio, and the degree of distinguishability of photons emitted by the two NV centers. We fix most parameters in our model using independent measurements, as described below, and fit for the visibility of the HOM interference. This visibility, which is extracted from the value of $g^{(2)}(0)$, is a measure of the indistinguishability of the photon pairs. Ideally, $g^{(2)}(0) = 0$ for a pair of indistinguishable photons, but the minimal observable $g^{(2)}(0)$ value increases in the presence of experimental noise, as

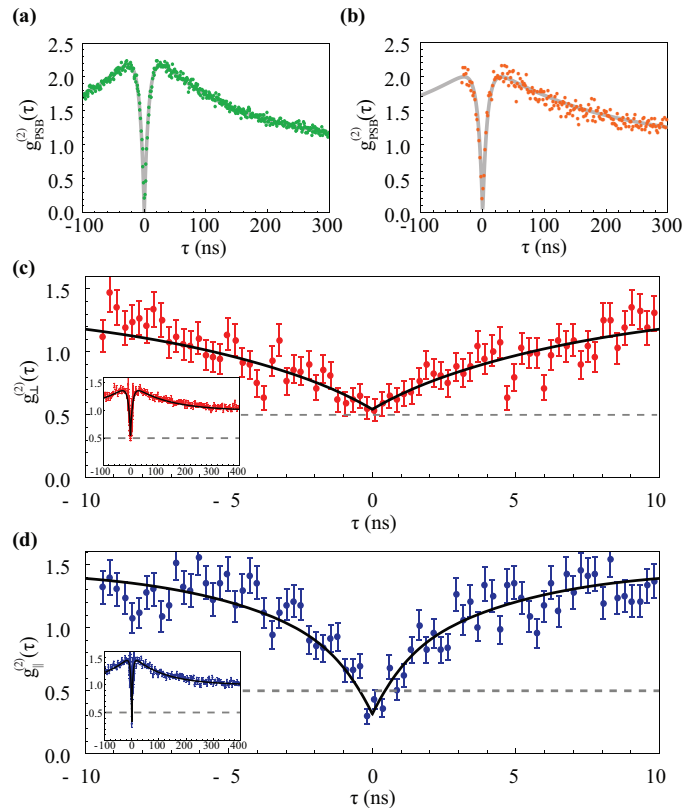


FIG. 3. (a,b) Single emitter second-order autocorrelation functions, $g_{\text{PSB}}^{(2)}(\tau)$, of the PSB emission, inferred for the two NV centers used for the HOM measurement. (c,d) Demonstration of HOM interference from remote NV centers in the (c) distinguishable case and (d) indistinguishable case. The dashed lines indicate the limit expected from independent distinguishable single photon sources at $\tau = 0$. Solid lines are a fit to the data based on the model described in the text. Error bars are estimated based on shot noise. The data is recorded with 64 ps bins, but for presentation has been binned to 192 ps for $|\tau| < 10$ ns and 3.84 ns bins for $|\tau| > 10$ ns. The data is independently analyzed for both 64 ps bins, and 192 ps bins and the parameter estimates for the fits are in very good agreement.

described below. When the photons are distinguishable and the light intensity in both arms is balanced, the correlation measurement will yield $g^{(2)}(0) = 0.5$ [11]. Measuring the cross-correlation function in the distinguishable case is equivalent to measuring the autocorrelation function of one emitter while the non-interfering emission from the other acts as uncorrelated noise, raising $g^{(2)}(0)$ from 0 to 0.5. Therefore, a measurement of $g^{(2)}(0) < 0.5$ indicates quantum interference between photons emitted by the two single photon sources.

Figures 3(c,d) show $g^{(2)}(0)$ for two different settings of the HWP angle. In Fig. 3(c), the angle is selected such that the emissions from the two NV centers are distinguished by their polarization, yielding $g_{\perp}^{(2)}(0) = 0.52 \pm$

0.04. In Fig. 3(d), the photons are indistinguishable when their polarizations are parallel, yielding $g_{||}^{(2)}(0) = 0.34 \pm 0.04$. In terms of the visibility of the HOM interference, defined as $\eta = [g_{\perp}^{(2)}(0) - g_{||}^{(2)}(0)]/g_{\perp}^{(2)}(0)$, we find $\eta = 35 \pm 9\%$. This $\eta > 0$ clearly demonstrates quantum interference between photons emitted by two NV centers separated by 2 m.

We next turn to the detailed discussion of our experimental observations. We first consider the sources of noise that will cause our result to deviate from the ideal case $g_{||}^{(2)}(0) = 0$. The APD dark counts and fluorescence background from our samples will lead to coincidence events, independent of the emission from the NV centers. Background light and the dark counts of our detectors contribute 80 cps out of the total 1100 cps signal, raising $g_{||}^{(2)}(0)$ to 0.14. Because the NV center spin is not perfectly polarized under green illumination [24], we expect to collect emission from other transitions (e.g. $|A_2\rangle$ to $|m_s = \pm 1\rangle$); since this emission is assumed to be circularly polarized, it is only partially filtered by the polarizer. Emission from other transitions at different frequencies raises the value of $g_{||}^{(2)}(0)$ by 0.07. Finally the polarization-maintaining fiber-based beamsplitters introduce rotations to the polarization of the emission, which increases the distinguishability of the two photons. This contribution raises the $g_{||}^{(2)}(0)$ value by another 0.07. Considering these factors, we expect experimental imperfections to raise $g_{||}^{(2)}(0)$ value to 0.29, which is in a very good agreement with our experimental observations.

The behavior of the measured $g_{||}^{(2)}(\tau)$ for τ longer than $1/\gamma$, where γ is the inverse lifetime of the emitter, is determined solely by the autocorrelation functions for the individual emitters. Using the model described in [28], we extract parameters from the two-emitter cross-correlation datasets [Figs. 3(c,d)] that are in good agreement with those extracted from the single-emitter autocorrelation datasets [Figs. 3(a,b)]. The HOM interference only occurs within a window around $\tau = 0$ whose width is determined by the bandwidth of the photons emitted from each NV center. In our model, we assume that the emission from the two NV centers is radiatively broadened with bandwidth $\sim \gamma$, and that the center frequencies of the emitted photons are random and different for subsequent emissions. We assume the distribution of the center frequencies is given by the Lorentzian profile that we fit to the absorption spectra shown in Fig. 2. Thus the HOM interference has an expected $1/e$ fullwidth of 2.4 ns. We find that the estimated width agrees with our measured data.

In summary, we have demonstrated the generation of indistinguishable photons from two spatially separated NV centers. Combined with the recent demonstration of entanglement between the electronic spin of an NV cen-

ter and the polarization of a photon [16], our work paves the way for optically mediated generation of entanglement between remote solid-state quantum registers. The techniques demonstrated here have yielded improved collection efficiency, control of the NV centers' optical transition frequencies via electric field tuning, and the ability to operate two independent setups simultaneously over three days of continuous data acquisition. The important figure of merit for an entanglement experiment is the time required to generate an entangled pair with fidelity greater than 50%. Considering the resonant excitation scheme used in [16], and noting that it will likely result in stable and narrow optical linewidths [22], we estimate that one entangled spin pair can be created within roughly ten seconds. Improved photon collection techniques that are currently being developed [29] have the potential to increase this generation rate dramatically. Even with the currently estimated rates, though, the exceptionally long nuclear spin memory times of NV centers [30] may allow one to use such systems for the realization of solid-state, multi-node quantum networks.

We thank N. de Leon, J. D. Thompson, R. Hanson, and L. Childress for useful discussions. This work was supported by NSF, CUA, DARPA QUEST program, AFOSR MURI, and Packard Foundation. A.K. acknowledges support from the Alexander von Humboldt Foundation.

* kubanek@fas.harvard.edu

- [1] C. Hong, Z. Ou, and L. Mandel, Phys. Rev. Lett. **59**, 2044 (1987).
- [2] Z. Ou, *Multi-Photon Quantum Interference* (Springer, 2007).
- [3] C. Santori, D. Fattal, J. Vučković, G. Solomon, and Y. Yamamoto, Nature (London) **419**, 594 (2002).
- [4] T. Legero, T. Wilk, M. Hennrich, G. Rempe, and A. Kuhn, Phys. Rev. Lett. **93**, 70503 (2004).
- [5] A. Kiraz, M. Ehrl, T. Hellere, Ö. Müstecaplıoğlu, C. Bräuchle, and A. Zumbusch, Phys. Rev. Lett. **94**, 223602 (2005).
- [6] L.-M. Duan and C. Monroe, Rev. Mod. Phys. **82**, 1209 (2010).
- [7] J. Beugnon, M. Jones, J. Dingjan, B. Darquie, G. Messin, A. Browaeys, and P. Grangier, Nature (London) **440**, 779 (2006).
- [8] P. Maunz, D. L. Moehring, S. Olmschenk, K. C. Younge, D. N. Matsukevich, and C. Monroe, Nat. Phys. **3**, 538 (2007).
- [9] D. Moehring, P. Maunz, S. Olmschenk, K. Younge, D. Matsukevich, L.-M. Duan, and C. Monroe, Nature (London) **449**, 68 (2007).
- [10] H. Bernien, L. Childress, L. Robledo, M. Markham, D. Twitchen, and R. Hanson, arXiv:1110.3329v1 (2011).
- [11] R. Lettow, Y. L. A. Rezus, A. Renn, G. Zumofen, E. Ikonen, S. Götzinger, and V. Sandoghdar, Phys. Rev. Lett. **104**, 123605 (2010).

- [12] E. B. Flagg, A. Muller, S. V. Polyakov, A. Ling, A. Migdall, and G. S. Solomon, *Phys. Rev. Lett.* **104**, 137401 (2010).
- [13] R. Patel, A. Bennett, I. Farrer, C. Nicoll, D. Ritchie, and A. Shields, *Nature Photon.* **4**, 632 (2010).
- [14] L. Childress, J. M. Taylor, A. S. Sørensen, and M. D. Lukin, *Phys. Rev. Lett.* **96**, 070504 (2006).
- [15] M. V. G. Dutt, L. Childress, L. Jiang, E. Togan, J. Maze, F. Jelezko, A. S. Zibrov, P. R. Hemmer, and M. D. Lukin, *Science* **316**, 1312 (2007).
- [16] E. Togan, Y. Chu, A. S. Trifonov, L. Jiang, J. Maze, L. Childress, M. V. G. Dutt, A. S. Sørensen, P. R. Hemmer, A. S. Zibrov, and M. D. Lukin, *Nature (London)* **466**, 730 (2010).
- [17] T. Babinec, B. Hausmann, M. Khan, Y. Zhang, J. Maze, P. Hemmer, and M. Lončar, *Nat. Nanotechnol.* **5**, 195 (2010).
- [18] A. Faraon, P. Barclay, C. Santori, K. Fu, and R. Beausoleil, *Nature Photon.* **5**, 301 (2011).
- [19] D. Englund, B. Shields, K. Rivoire, F. Hatami, J. Vučković, H. Park, and M. D. Lukin, *Nano. Lett.* **10**, 3922 (2010).
- [20] R. Kolesov, B. Grotz, G. Balasubramanian, R. J. Stohr, A. A. L. Nicolet, P. R. Hemmer, F. Jelezko, and J. Wrachtrup, *Nat. Phys.* **5**, 470 (2009).
- [21] P. Siyushev, F. Kaiser, V. Jacques, I. Gerhardt, S. Bischof, H. Fedder, J. Dodson, M. Markham, D. Twitchen, F. Jelezko, *et al.*, *Appl. Phys. Lett.* **97**, 241902 (2010).
- [22] K.-M. C. Fu, C. Santori, P. E. Barclay, L. J. Rogers, N. B. Manson, and R. G. Beausoleil, *Phys. Rev. Lett.* **103**, 256404 (2009).
- [23] P. Tamarat, T. Gaebel, J. Rabeau, M. Khan, A. Greentree, H. Wilson, L. Hollenberg, S. Prawer, P. Hemmer, F. Jelezko, *et al.*, *Phys. Rev. Lett.* **97**, 83002 (2006).
- [24] N. Manson, L. Rogers, M. Doherty, and L. Hollenberg, *arXiv:1011.2840v1* (2011).
- [25] A. Batalov, V. Jacques, F. Kaiser, P. Siyushev, P. Neumann, L. J. Rogers, R. L. McMurtrie, N. B. Manson, F. Jelezko, and J. Wrachtrup, *Phys. Rev. Lett.* **102**, 195506 (2009).
- [26] L. Bassett, F. Heremans, C. Yale, B. Buckley, and D. Awschalom, *arXiv:1104.3878v1* (2011).
- [27] J. Maze, A. Gali, E. Togan, Y. Chu, A. Trifonov, E. Kaxiras, and M. D. Lukin, *New J. Phys.* **13**, 025025 (2011).
- [28] C. Kurtsiefer, S. Mayer, P. Zarda, and H. Weinfurter, *Phys. Rev. Lett.* **85**, 290 (2000).
- [29] I. Aharonovich, A. D. Greentree, and S. Prawer, *Nat. Photon.* **5**, 397 (2011).
- [30] P. C. Maurer, *et al.*, “Room temperature solid-state quantum bit with second-long memory”(To be published).